Interfacial Films

International Edition: DOI: 10.1002/anie.201603706
German Edition: DOI: 10.1002/ange.201603706

Design of Highly Stable Echogenic Microbubbles through Controlled Assembly of Their Hydrophobin Shell

Lara Gazzera, Roberto Milani, Lisa Pirrie, Marc Schmutz, Christian Blanck, Giuseppe Resnati, Pierangelo Metrangolo, and Marie Pierre Krafft**

Abstract: *Dispersing hydrophobin HFBII under air saturated with perfluorohexane gas limits HFBII aggregation to nanometer-sizes. Critical basic findings include an unusual co-adsorption effect caused by the fluorocarbon gas, a strong acceleration of HFBII adsorption at the air/water interface, the incorporation of perfluorohexane into the interfacial film, the suppression of the fluid-to-solid 2D phase transition exhibited by HFBII monolayers under air, and a drastic change in film elasticity of both Gibbs and Langmuir films. As a result, perfluorohexane allows the formation of homogenous populations of spherical, narrowly dispersed, exceptionally stable, and echogenic microbubbles.*

Microbubbles are currently used and further investigated for contrast ultrasound (US) imaging, molecular imaging, targeted drug and gene delivery, and as mechanical intravascular intervention devices.[1] There is, however, a clear need for innovative microbubble shell components. The existing ones, phospholipids and polymers, only poorly meet the essential requirements for US contrast agent (USCA) microbubbles, which need to be simultaneously highly echogenic, stable, and size-controlled.[2] Phospholipid-stabilized microbubbles have a thin (tens of nm), highly echogenic shell, but they need to be prepared just prior to use from freeze-dried materials.[3] On the other hand, polymer-stabilized microbubbles are stable for months, but their shell is much thicker (a few hundreds of nm), which dampens the US waves and considerably decreases echogenicity at low US pressures. At high acoustic pressures, the polymer microbubbles break and the internal gas escapes.

Hydrophobins (HFBs) are small fungal amphiphilic proteins with remarkable surface activity.[4] HFBII (Figure 1 a), obtained from *Trichoderma reseei*, forms ordered monolayers at interfaces, which is potentially valuable for bubble and foam stabilization in the food industry. HFBII was reported to stabilize inorganic and polymer nanoparticles and fluorocarbon emulsions in water.[5]

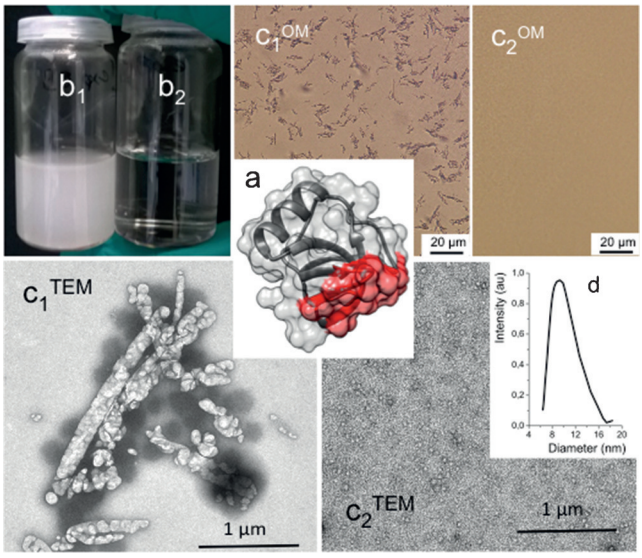

Figure 1. a) HFBII (2×2×3 nm, hydrophobic patch in red). b) Shear-mixed aqueous dispersions of HFBII under air (b_1) and *F*-hexane-saturated air (b_2). c) Morphology of aggregates formed in aqueous dispersions of HFBII under air (c_1) and *F*-hexane-saturated air (c_2); ^{OM}optical microscopy (on shear-mixed samples), ^{TEM}TEM (negative staining, on samples before shear mixing). d) Diameter distribution of aggregates in HFBII dispersions in contact with *F*-hexane (DLS). HFBII concentration, 0.2 mg mL^{-1}; room temperature.

We have investigated HFBII as a microbubble shell component for medical US imaging. HFBII Gibbs monolayers adsorbed at the air/water interface are known to exhibit a concentration-dependent transition from a fluid to a 2D solid state, resulting in high shear elasticity.[6] While microbubble stability is essential for use as USCA, excessive elasticity is expected to shift the bubble's resonance frequency to high values[7] that may exceed those commonly used in radiology (that is, from 2 to 15 MHz). Another consequence of HFBII monolayers being in a solid state is that millimetric[8] and micrometric[9] HFBII-stabilized bubbles adopt elongated shapes. Dispersions containing both elongated and spherical microbubbles are suboptimal as USCA since microbubble resonance frequency depends on the radius.[10] Finally, some feasibility tests showed that dispersing HFBII and preparing microbubbles using standard procedures leads to heterogeneous mixtures consisting largely of micron-sized aggregates along with both spherical and elongated microbubbles (see below), thus impeding the

[*] Dr. L. Gazzera, Prof. G. Resnati, Prof. P. Metrangolo
NFMLab
Politecnico di Milano
Via Mancinelli 7, 20131 Milano (Italy)
E-mail: pierangelo.metrangolo@polimi.it
Dr. R. Milani, Dr. L. Pirrie, Prof. P. Metrangolo
VTT-Technical Research Centre of Finland Ltd
Biologinkuja 7, Espoo, 02044 VTT (Finland)
Dr. M. Schmutz, C. Blanck, Dr. M. P. Krafft
Institut Charles Sadron (CNRS), University of Strasbourg
23 rue du Loess, 67034 Strasbourg (France)
E-mail: krafft@unistra.fr

Supporting information for this article can be found under: http://dx.doi.org/10.1002/anie.201603706.

reproducible and effective formation of echogenic microbubbles.

Herein, we report that both the HFBII dispersion issue and the conflicting microbubble stability/elasticity requirements can be solved by using a fluorocarbon (*F*C) gas (perfluorohexane, *F*-hexane). Size- and shape-controlled populations of stable echogenic microbubbles could thus be obtained. Both HFBII and the *F*C gas are expected to be biologically inert.[11,12] First, we report that *F*-hexane prevents the protein from forming large aggregates when dispersed in water. Moreover, the fluid-to-solid transition in HFBII Langmuir monolayers can be inhibited by the *F*C gas, allowing the monolayers to remain fluid throughout compression. Likewise, Gibbs interfacial films are fluid at high protein concentrations. In the fluid state, the HFBII adsorption kinetics at the air/water interface, as determined by bubble profile analysis tensiometry, is greatly accelerated when *F*-hexane is introduced in the gas phase. While micrometric air-only HFBII bubbles are elongated and not echogenic in the investigated frequency range (0.3–6.6 MHz), introducing *F*-hexane produces only spherical bubbles. These findings support a new approach to controlling 1) the aggregation behavior of HFBII in water and 2) the morphology, stability, and echogenic response of HFBII-shelled microbubbles and open new outlooks for medical microbubble development. In fact, most microbubbles currently used or investigated for US diagnosis and drug delivery contain *F*C gases.[1]

*F*C gases have also promising applications in lung therapy[13] and for biomarker recognition and immobilization.[14]

The preparation of microbubbles first involves the low-energy dispersion in water of the shell-forming HFBII, followed by a more energetic mechanical agitation (see the Supporting Information). First, we wanted to assess the effect of *F*-hexane on HFBII dispersion characteristics. When dispersed in water by shear mixing under air in a rotary shaker, a highly purified sample of HFBII formed a milky dispersion (Figure 1 b_1) containing fibrils large enough (2–3 μm in diameter, up to 20–30 μm in length) to be seen by optical microscopy (Figure 1 c_1^{OM}).[9,15] Transmission electron microscopy (TEM, negative staining) on the HFBII dispersions shows aggregates with a rod-like convoluted morphology even before shear mixing (Figure 1 c_1^{TEM}).

By contrast, when the HFBII dispersions are prepared under *F*-hexane-saturated air, the dispersions are transparent and no large aggregates are seen by optical microscopy (Figures 1 b_2,c_2^{OM}). Only nano-sized aggregates (ca. 8–12 nm, tens of molecules) were observed by TEM (Figure 1 c_2^{TEM}), showing that *F*-hexane completely prevents the formation of the large aggregates. The diameter of the HFBII nanoaggregates was confirmed by dynamic light scattering (DLS); (Figure 1 d). Notably, the initial large, micron-sized aggregates formed in the absence of *F*-hexane reappear when *F*-hexane is replaced by air.

We compared the formation of microbubbles from HFBII dispersions prepared under air or prepared and stored under *F*-hexane-saturated air. In both cases, the dispersions, which were not subjected to shear mixing, were transparent. Under air, three kinds of diversely sized objects were identified in the microbubble samples: 1) rod-shaped micron-sized aggregates like those found in HFBII dispersions, 2) spherical microbubbles, and 3) elongated microbubbles (Figure 2 a, Table 1). 80 % of the objects were elongated (circularity below 0.3; see the Supporting Information for image analysis). Attempts to separate elongated and spherical objects using flotation failed.

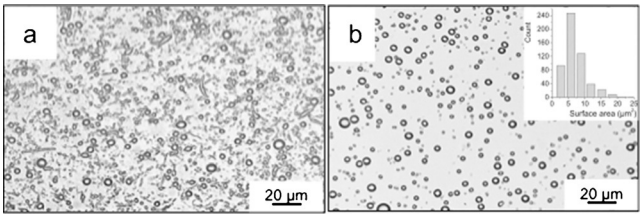

Figure 2. Dispersions of HFBII in water obtained by mechanical agitation under a) air or b) air saturated with *F*-hexane, as assessed by optical microscopy. Inset: Diameter distribution of microbubbles found in (b) as assessed by optical microscopy. HFBII concentration, 0.2 mg mL^{-1}; room temperature.

Table 1: Morphological characteristics of aggregates and microbubbles found in aqueous HFBII dispersions as determined by optical microscopy.

HFBII dispersions	Spherical microbubbles[a]		Elongated objects[b] (aggregates or bubbles)	
	%	Diameter [μm]	%	Length [μm]
Under air	20	5	80	8–10
Under *F*-hexane	98	2–3	2	–

[a,b] Objects for which the circularity is [a] > 0.90 and [b] < 0.30.

Using *F*-hexane-saturated air during microbubble preparation changes the situation radically. Essentially all the elongated objects disappear and only spherical bubbles are formed (> 98 %); (Figure 2 b, Table 1). No solid aggregates are seen.

The acoustic behavior of the microbubbles was studied by measuring the attenuation coefficient α of US waves that propagate through a bubble dispersion as a function of time for a range of US frequencies *f*. Contrary to those prepared under air, the *F*-hexane-stabilized bubbles were highly echogenic, with α values close to those of phospholipid-shelled microbubbles.[16] Figure 3 a shows the variation of α as a function of *f* at the initial time t_0. The bubble size distributions (Figure 3 b), as determined from the US absorption spectra, show monomodal populations (diameter, 6.2 ± 1.6 μm; polydispersity index PI, 25 %). 50 % of the bubbles were still present in the US measuring cell after nearly 4.5 h (Figure 3 c). Decisively, it then became possible to fractionate the microbubble population by flotation. Thus, a narrowly dispersed population of microbubbles (mean diameter, 3.7 ± 0.9 μm; PI, 24 %) could be obtained, as assessed by optical microscopy, static light scattering (SLS), and the acoustical attenuation method (Figure 3 d).[16]

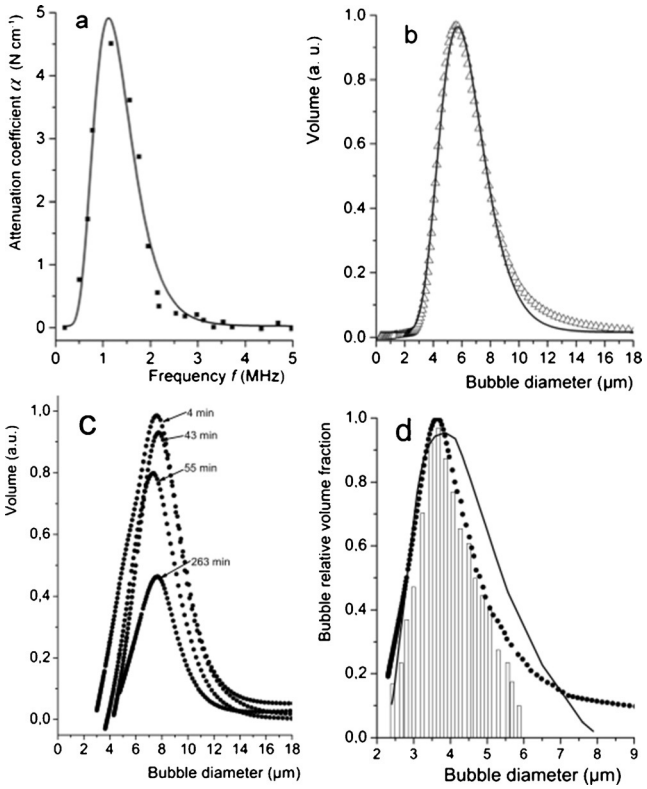

Figure 3. a) Variation of the attenuation coefficient α as a function of ultrasound frequency *f* for microbubbles prepared from HFBII dispersions under *F*-hexane; b) microbubble distributions from the US absorption spectra; c) time evolution of the bubble distributions (acoustical method); d) size distributions of the fractionated *F*-hexane-stabilized HFBII microbubbles, assessed by optical microscopy (bars), SLS (line), and US attenuation measurements (filled circles). Mean diameter $\approx$ 3.5 μm. HFBII concentration, 0.2 mg mL^{-1}; injected volume 1 mL; 25 °C.

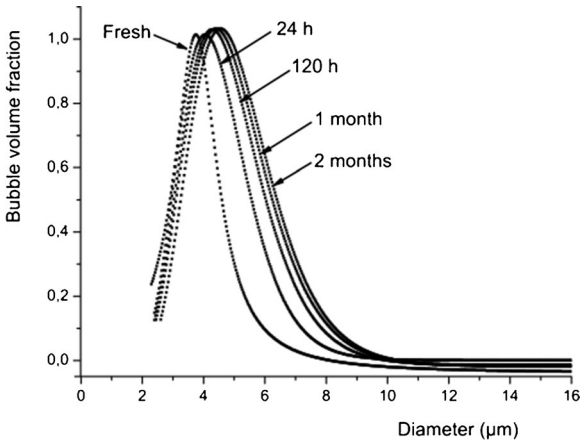

Figure 4. Size distribution of an *F*-hexane-stabilized HFBII microbubble dispersion as measured acoustically after 5 min of flotation, and after 24 h, 48 h, 120 h, and 1 and 2 months at room temperature. HFBII concentration, 0.2 mg mL^{-1}.

By contrast, HFBII microbubbles prepared without *F*-hexane were, as anticipated, poorly echogenic, with α coefficients up to 20-fold lower than those obtained with the *F*C (Supporting Information, Figures S1–2). This is likely a result of the presence of a large concentration of non-echogenic solid aggregates and of the high polydispersity of the microbubble sizes and curvatures.

F-hexane also has a strong effect on the microbubble stability. The HFBII-shelled bubbles prepared under air last approximately 15 min at 25 °C (Supporting Information, Figure S1). Previously, HFBII microbubbles have been reported that last for several days.[9] The difference in stability may be related to differences in the HFBII sample purity (higher in our case), air phase volume (lower in our case), and ratio of elongated bubbles (higher in our case).

In contrast, microbubbles prepared and stored under *F*-hexane, after an initial shift toward a slightly larger diameter (ca. 4.5 μm), display a mean diameter and a size distribution that remain essentially unchanged for at least 2 months at 25 °C (Figure 4; SLS in the Supporting Information, Figure S3).

The simultaneous presence of hydrophobin and *F*-hexane in the bubble shell was established by FTIR, which showed the simultaneous characteristic vibrations (cm^{-1}) of HFBII amide C=O (1623) and *F*-hexane C–F (1201, 1148); (Supporting Information, Figure S4).

We investigated Gibbs films of HFBII adsorbed at the air (or *F*-hexane-saturated air)/water interface using bubble profile analysis tensiometry. At high HFBII concentrations, the measurement of the surface tension σ is not valid because, for an elastic solid film, σ becomes an anisotropic quantity.[6] As a consequence, the error on the Laplace fit becomes prohibitively high.[6] By contrast, under *F*-hexane the errors on the fit remain small (Figure 5), implying that the HFBII

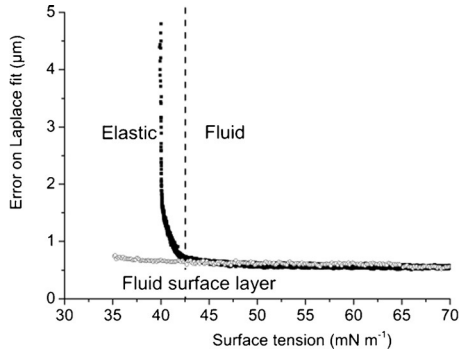

Figure 5. Error on the fit of the drop profile using the Laplace equation versus surface tension, as determined by bubble profile analysis. The abrupt increase observed at low σ values reflects the fluid-to-elastic transition of the HFBII layer adsorbed at the air/water interface (filled squares). On the other hand, when *F*-hexane is present, the errors remain small, showing that the HFBII layer remains fluid (open circles). HFBII concentration, 0.05 mg mL^{-1}; 25 °C.

layer remains fluid at all surface pressures. The effect of *F*-hexane on spontaneous HFBII adsorption was therefore investigated at protein concentrations at which the layer at equilibrium is in the fluid state (0.01 mg mL^{-1}, Figure 6).

F-hexane was found to strongly accelerate the adsorption of the protein (characteristic time $\tau = 130$ s versus 421 s in its

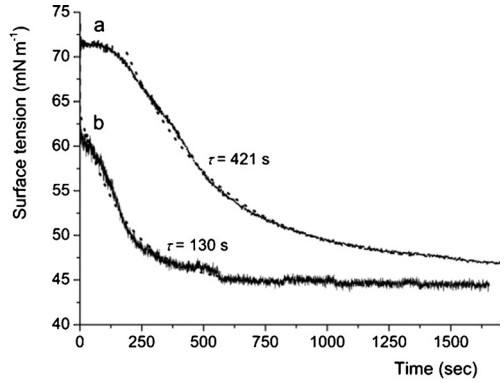

Figure 6. Adsorption kinetics of hydrophobin HFBII (0.01 mg mL^{-1}; 25 °C) at the interface of water and air (a), or *F*-hexane-saturated air (b), as determined by tensiometry. The characteristic adsorption times τ (±50 s) were obtained by fitting the experimental curves with an exponential decay function (dotted lines).

absence). This is likely due to *F*-hexane's ability to limit protein aggregation to nanometer-sized entities that diffuse faster to the interface. The *F*C was also found to decrease the equilibrium interfacial tension of HFBII by approximately 3–4 mN m^{-1}, which shows the co-adsorption of the two compounds at the interface (Figure 6). Most importantly, *F*-hexane significantly decreases the viscoelastic modulus *E* of the surface film (from 138.1 ± 8.2 to 102.5 ± 3.8 mN m^{-1}).

We studied Langmuir compression isotherms to assess the co-adsorption of HFBII and *F*-hexane in interfacial films. HFBII monolayers were spread over water in a trough enclosed in a gas-tight box, allowing the saturation of the gas phase with *F*-hexane.[13] Under air, HFBII monolayers exhibit a fluid-to-solid transition[6] when approaching a surface pressure (π) of approximately 20 mN m^{-1} (Figure 7). By contrast, when the monolayers are in contact with *F*-hexane, the isotherm is shifted towards larger surface areas, implying that the *F*C molecules are inserted in the monolayer and act as a co-surfactant. This is reminiscent of the fluidizing effect exerted by *F*C gases on phospholipid monolayers[13] At higher surface pressures the area difference with and without *F*-hexane decreases, but is not reduced to zero, suggesting that the *F*C is only partially expelled from the monolayer. The collapse pressure of the monolayer in contact with *F*-hexane is also notably higher (ca. 60 versus ca. 54 mN m^{-1}) than in its absence.

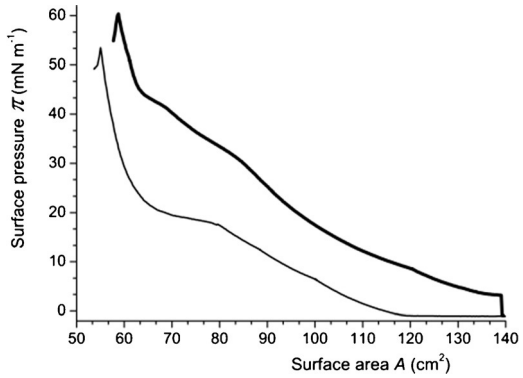

Figure 7. Surface pressure (π)/surface area (A) isotherms (25 °C) of HFBII monolayers compressed under air (thin line) and *F*-hexane-saturated air (thick line).

In summary, in the absence of *F*-hexane, shear-mixed HFBII dispersions consist of highly heterogeneous populations of large, solid, mostly elongated aggregates. As a result, HFBII microbubbles are polymorphous and polydisperse. Moreover, the fluid-to-highly elastic solid-phase transition in monolayers precludes microbubbles to be echogenic in the 0.3–6.6 MHz range. These deficiencies hamper the development of effective medical microbubbles. We found that these obstacles can be removed and that bubble stability and echogenicity can be greatly increased, by introducing *F*-hexane in the gaseous phase. *F*-hexane limits protein aggregation to nanometer-scale sizes. Most importantly, contact with *F*-hexane prevents the formation of the HFBII 2D solid phase. Consequently, exposure to *F*-hexane enables the efficient, quasi-exclusive formation of homogenous, narrowly dispersed populations of spherical stable and echogenic microbubbles. This may be because 1) the nanometer-sized aggregates diffuse more rapidly to the interface and stabilize microbubbles more efficiently and 2) *F*-hexane is immobilized in the bubble's shell, maintaining its fluidity and therefore enabling effective bubble resonance when insonified in a frequency range commonly utilized in US imaging. *F*-hexane thus allows the production of microbubbles that are compatible with medical uses. More generally, we believe that these results should facilitate the use of these intriguing amphiphilic proteins in soft matter and interfacial science.

Acknowledgements

We thank the French National Research Agency (ANR-14-CE35-0028-01), the Academy of Finland (276537.284508.260565), the French Institute of Finland for funding, and Teclis Instruments (Longessaigne, France) for discussions and technical support. Part of the experimental work was done by L. G., R. M., and L. P. during their stay at the Institut Charles Sadron, Strasbourg.

Keywords: echogenicity · fluorocarbons · hydrophobin · interfacial films · ultrasound imaging

How to cite: *Angew. Chem. Int. Ed.* **2016**, *55*, 10263–10267
Angew. Chem. **2016**, *128*, 10419–10423

[1] E. Unger, T. Porter, J. Lindner, P. Grayburn, *Adv. Drug Delivery Rev.* **2014**, *72*, 110–126.
[2] S. R. Sirsi, M. A. Borden, *Adv. Drug Delivery Rev.* **2014**, *72*, 3–14.
[3] S. Unnikrishnan, A. L. Klibanov, *Am. J. Roentgenol.* **2012**, *199*, 292–299.
[4] M. B. Linder, *Curr. Opin. Colloid Interface Sci.* **2009**, *14*, 356–363.
[5] a) A. Schulz, B. M. Liebeck, D. John, A. Heiss, T. Subkowski, A. Böker, *J. Mater. Chem.* **2011**, *21*, 9731–9736; b) R. Milani, E. Monogioudi, M. Baldrighi, G. Cavallo, V. Arima, L. Marra, A. Zizzari, R. Rinaldi, M. Linder, G. Resnati, P. Metrangolo, *Soft Matter* **2013**, *9*, 6505–6514; c) C. Pigliacelli, A. D'Elicio, R.

Milani, G. Terraneo, G. Resnati, F. Baldelli Bombelli, P. Metrangolo, *J. Fluorine Chem.* **2015**, *177*, 62 – 69.
[6] N. A. Alexandrov, K. G. Marinova, T. D. Gurkov, K. D. Danov, P. A. Kralchevsky, S. D. Stoyanov, T. B. J. Blijdenstein, L. N. Arnaudov, E. G. Pelan, A. Lips, *J. Colloid Interface Sci.* **2012**, *376*, 296 – 306.
[7] T. van Rooij, Y. Luan, G. Renaud, A. F. W. van der Steen, M. Verluis, N. de Jong, K. Kooiman, *Ultrasound Med. Biol.* **2015**, *41*, 1432 – 1445.
[8] E. S. Basheva, P. A. Kralchevsky, N. C. Christov, K. D. Danov, S. D. Stoyanov, T. B. J. Blijdenstein, H.-J. Kim, E. G. Pelan, A. Lips, *Langmuir* **2011**, *27*, 2382 – 2392.
[9] A. R. Cox, F. Cagnol, A. B. Russell, M. J. Izzard, *Langmuir* **2007**, *23*, 7995 – 8002.
[10] M. A. Parrales, J. M. Fernandez, M. Perez-Saborid, J. A. Kopechek, T. M. Porter, *J. Acoust. Soc. Am.* **2014**, *136*, 1077 – 1084.
[11] a) J. G. Riess, *Chem. Rev.* **2001**, *101*, 2797 – 2920; b) S. F. Flaim, *Artif. Cells Blood Substitutes Immobilization Biot* **1994**, *22*, 1043 – 1054.
[12] a) M. Sarparanta, L. M. Bimbo, J. Rytkönen, E. Mäkilä, T. J. Laaksonen, P. Laaksonen, M. Nyman, J. Salonen, M. B. Linder, J. Hirvonen, H. A. Santos, A. J. Airaksinen, *Mol. Pharm.* **2012**, *9*, 654 – 663; b) M. I. Janssen, M. B. M. van Leeuwen, K. Scholtmeijer, T. G. van Kooten, L. Dijkhuizen, H. A. B. Wösten, *Biomaterials* **2002**, *23*, 4847 – 4854; c) V. Aimanianda, J. Bayry, S. Bozza, O. Kniemeyer, K. Perruccio, S. R. Elluru, C. Clavaud, S. Paris, A. A. Brakhage, S. V. Kaveri, L. Romani, J.-P. Latge, *Nature* **2009**, *460*, 1117 – 1121; d) Q. Ren, A. H. Kwan, M. Sunde, *Pept. Sci.* **2013**, *100*, 601 – 612.
[13] F. Gerber, M. P. Krafft, T. F. Vandamme, M. Goldmann, P. Fontaine, *Angew. Chem. Int. Ed.* **2005**, *44*, 2749 – 2752; *Angew. Chem.* **2005**, *117*, 2809 – 2812.
[14] G. Yang, M. O'Duill, V. Gouverneur, M. P. Krafft, *Angew. Chem. Int. Ed.* **2015**, *54*, 8402 – 8406; *Angew. Chem.* **2015**, *127*, 8522 – 8526.
[15] M. Torkkeli, R. Serimaa, O. Ikkala, M. Linder, *Biophys. J.* **2002**, *83*, 2240 – 2247.
[16] S. Rossi, G. Waton, M. P. Krafft, *Langmuir* **2010**, *26*, 1649 – 1655.

Received: April 17, 2016
Revised: May 19, 2016
Published online: July 27, 2016

